Publishing House
AKAPIT

COMPUTER METHODS IN MATERIALS SCIENCE

Informatyka w Technologii Materiałów

Vol. 12, 2012, No. 1

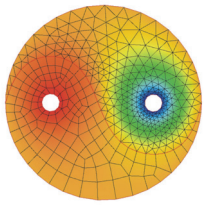

AN EVALUATION OF THROUGH-THICKNESS DEFORMATION MECHANISMS IN SINGLE POINT INCREMENTAL SHEET FORMING USING A DUAL-LEVEL FINITE-ELEMENT MODEL

KHAMIS ESSA, PETER HARTLEY*

School of Mechanical Engineering, College of Engineering and Physical Sciences
University of Birmingham, Edgbaston, Birmingham, B15 2TT, UK
**Corresponding author: phartley2009@gmail.com*

Abstract

Single point incremental forming (SPIF) is a process with the capability to form complex geometries using a tool of very simple geometry, without the need for a matching die. At present, through-thickness modes of deformation and the existence of through-thickness shear are not clear. The objectives of this report are firstly, to establish a computational methodology to study the deformation mechanism of SPIF and secondly, to provide a clear description of the deformation modes that take place through the sheet thickness. The methodology is, in essence, a multi-level approach, although in this example only two levels are necessary. In this paper, a 3-D implicit finite-element (FE) model of the complete sheet being formed, with two elements through the thickness and a second-level FE model of a smaller segment of the sheet, with seven elements through its thickness, are used in a dual-level approach. The results show that the full model is capable only of exploring the principal characteristics of the deformation, normal strains and the final product geometries. The second-level model demonstrates a capability to predict more accurately the deformation modes through the sheet thickness and shows the influence of tool friction and diameter on the through-thickness shear strains. A combination of bending, stretching and thinning modes of deformation in addition to through thickness shear is found. The results obtained provide a more complete description of through-thickness deformation mechanisms.

Key words: Asymmetric incremental sheet forming; Single point incremental forming; Finite element analysis; through-thickness deformation modes; shear strain

1. INTRODUCTION

Many industrial sectors use forming processes such as spinning, stamping and deep drawing in order to produce sheet metal components with high productivity. These processes require a high initial capital investment, long die-preparation times and dedicated dies for each part. Asymmetric incremental sheet forming (AISF) generally refers to an alternative die-less forming process which can be used to form complex shapes using simple tools. The process has received increasing attention due to its high flexibility and low cost and is especially valuable for low-volume specialised components. In AISF, a simple tool moves over the sheet surface and produces highly localised plastic deformation. Thus, a variety of complex 3-D shapes can be formed as the tool moves through carefully controlled paths. There are two types of asymmetric incremental forming referred to as two point incremental forming (TPIF) and single point incremental forming (SPIF). In this paper, only the SPIF configuration will be investigated, a schematic of which is shown in figure 1.

ISSN 1641-8581

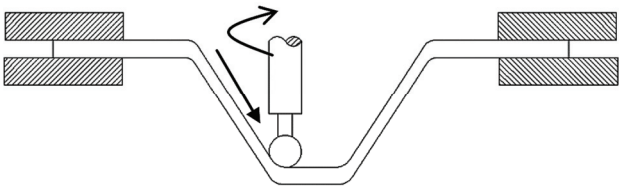

Fig. 1. *Single point incremental forming configuration.*

Knowledge of the process mechanics is crucial to understand how the final properties of the part made by AISF develop and to identify the process forming limits. Many of the previous investigations have focused on an analysis of deformation mechanics through experimental investigations or by using the finite element (FE) method. The work however, is contradictory with different views on the detailed deformation modes. In the analysis of stress and strain history reported by Bambach et al. (2003), Hirt et al. (2003) and later Ambrogio et al. (2004), it was suggested that stretching and thinning are the dominant modes of deformation and all shear strain components through the thickness are negligible. Conversely, the experimental measurements of Allwood et al. (2007) indicated that high values of transverse shear are present through the thickness. Jackson and Allwood (2009) also showed experimentally a significant value of through-thickness shear in two planes. One of these planes is perpendicular to the tool movement and the other is parallel to the tool direction. It has been suggested that this shear strain could be a major contribution to the increase in the forming limit of the material in this process. A useful review of alternative mechanisms that might explain the enhanced formability of AISF has been provided by Emmens and Van Den Boogaard (2009), where descriptions of the contributions of aspects such as contact stress, bending-under-tension, cyclic straining and hydrostatic stress, as well as through-thickness shear, are given. However, the focus of the current paper is on providing an alternative means of determining through-thickness shear strain.

The complex nature of the deformation results from many factors such as the continually changing contact location, large plastic deformation and complex tool kinematics. Numerical methods, for example FE modelling, permit a detailed study of this behaviour and as experimental observations of through-thickness phenomena are extremely difficult, modelling of the AISF processes becomes an essential tool. Jackson and Allwood (2009) suggested that an FE model with a large number of elements through the thickness must be used to accurately predict the strain on any element. The use of shell elements in the simulation of AISF may be limited since they cannot be used to predict fully all the through-thickness phenomena. They suggested that an implicit code would provide greater accuracy than the explicit approach.

Lasunon and Knight (2007) have conducted experimental and numerical investigations on both single point and two point incremental forming processes. The FE models used Abaqus/Explicit with shell elements to simulate and study the effects of process variables on the formed profiles and thickness variations for both processes. They concluded that for the pyramidal parts produced by SPIF, the greatest thinning took place at the corner of the part, whereas, for the same parts produced by TPIF, the greatest thinning occurred in the walls of the parts. For the same purpose, Dejardin et al. (2008) constructed finite element models, again using an explicit code and shell elements for SPIF. Additional experimentation, i.e. final shape measurements, was undertaken in order to validate the FE model. They concluded that the final product quality could be improved by accurately controlling the tool path.

Eyckens et al. (2007) constructed a partial FE model, using linear brick elements with Abaqus/Implicit, of a conical shape produced by SPIF, to predict the forming limit of the process. In this model, three elements were assigned through the sheet thickness in order to identify the strain path. It was reported that the deformation can be characterized as plane strain in the cone wall and stretching along the radial direction. A later report by Eyckens et al. (2008) used a sub-modelling technique with a local refined mesh. Tanaka et al. (2007) also constructed a partial model of an SPIF cone forming process to assess residual stress, although this single-level model consisted of a regular hexahedral segment with no influence of prior process deformation. Ma and Mo (2008) constructed full and simplified 3-D FE models for single point incremental forming to simulate the deformation of a truncated cone and a truncated pyramid. Both models used only one linear brick element through the thickness. They reported that although brick elements are much better than shell elements, the simulation time is much longer. They concluded that three different regions each with a different deformation pattern were found in the deformed part. However, the deformation in general is a combination of bending and stretching. Although these results agreed with the findings of Bambach et al. (2003), the use of one element

through the thickness is not sufficient to clarify all the deformation modes. Robert et al. (2008) introduced an elasto-plastic material definition implemented through a VUMAT user subroutine with shell elements to minimize the FE simulation time using Abaqus/Explicit. The objective was to implement the incremental deformation theory of plasticity. They concluded that this approach can improve the efficiency of the modelling process and reduce the computational time.

A number of mechanisms have been proposed to explain the enhanced formability associated with AISF processes as detailed in Emmens and Van Den Boogaard (2009). One of these theories which had not previously been numerically predicted is based on the existence of an enhanced through-thickness shear strain. In addition, an extended Marciniak-Kuczynski (MK) model framework was proposed by Eyckens (2010) in order to explicitly account for through-thickness shear. The extended MK model shows that through-thickness shear increases the forming limit and delays the onset of localised necking. In the current paper, a dual-level FE modelling technique has been used to predict the through-thickness deformation mechanism which is expected to have a significant influence on the formability in SPIF.

The previous investigations were carried out to study the effect of process parameters on the final product geometry and accuracy, and to validate the FE results. It is apparent that both the experimental and FE approaches do not provide sufficient detail of the through-thickness modes of deformation. For the published FE models, limitations are found in terms of the maximum number of elements through the thickness. Most of the FE models used an explicit code with shell elements to reduce the simulation time with an inherent reduction in the accuracy of the results.

In the present investigation a two-stage or dual-level approach is described in which a more detailed description of the deformation mechanics is provided. This is achieved initially through the use of a full 3-D FE model; in the example here SPIF is used to produce a truncated cone. The initial model of the complete sheet is performed using an implicit code (Abaqus) with two linear solid elements through the thickness. The objective of this is to predict the product geometry, normal strains and to provide general information on the process. The second stage of the modelling procedure is to interrupt the process simulation of the full model and create a more refined model of a smaller segment of the deforming sheet. This second model encompasses a region around the forming tool that includes deformed and un-deformed material. The geometry and boundary conditions of the new model are defined by the shape of the sheet at the point at which the process was interrupted. This is re-meshed with seven solid elements through the thickness. The aim of the new model is to explore the deformation mechanism of the process in greater detail and hence gain a clear description of the modes of deformation through the thickness of the sheet. The new dual-level approach provides an alternative to existing techniques with a greater level of detail and gives more detailed information on the behaviour of through-thickness shear in the SPIF process.

2. FINITE ELEMENT MODEL

The large plastic deformation and continuous change of tool-sheet contact location, inherent in SPIF provides a complex challenge for simulation. No conditions of symmetry may be assumed and thus, a full three dimensional FE model is required. The use of an implicit code will provide more reliable data on the stress and strain history but the simulation time is normally very long. In order to improve the accuracy of FE modelling, domain decomposition and forms of sub-structuring techniques have been proposed. Domain decomposition requires the model to be divided into a number of sub-domains, and the whole deformation model solved by parallel computing. The sub-domains maintain compatibility with each other by applying appropriate boundary conditions on the connecting interfaces. Such techniques are often applied in nonlinear computational mechanics, e.g. in the simulation of forming processes such as extrusion (Park & Yang, 2000) and spinning (Quigley & Monaghan, 2002). In domain decomposition, an overlap between explicit and implicit is possible. Hadoush and Van Den Boogaard (2008, 2009) proposed a special case of domain decomposition known as the sub-structuring method. The approach was applied to SPIF to reduce the computing time by entirely refining an intermediate coarse mesh. It consists of adapting the number of grid points and changing their connectivity. Grid points are added to areas where more accuracy is demanded and can be deleted in areas where the solution is sufficiently accurate.

Eyckens et al. (2010) applied a sub-modelling technique to SPIF that enabled a high mesh density

to be used in the small plastic zone under the forming tool with a reasonable computational cost. This technique starts with a large scale FE simulation of the process (the global model). The nodes initially in the vicinity of the boundary of the sub-model are identified before the simulation begins, and all their nodal displacements stored. This is followed by a second simulation using the model with a local refined area, which also starts from the un-deformed blank. Onto the edges of the sheet sub-model, displacement boundary conditions are imposed to ensure compatibility with the global model.

The technique proposed in the current paper has some similarities with the sub-modelling approach of Eyckens et al. (2010), but has the advantage that the whole process does not need to be simulated twice. The refined segment of the mesh is extracted from the original model in a deformed state, the geometry being obtained from the first-level analysis, and additional deformation in the second-level model sufficient only to provide details of the through-thickness strain distribution is required. An advantage over the domain decomposition approach is that the simulations can be performed with a single processor and can be used as an added feature to any commercial FE package. The dual-level approach is described in section 4.

2.1. Sheet geometry and material properties

A rectangular sheet with an edge length of 170 mm by 170 mm and thickness of 1 mm is used to produce a truncated cone that has a wall angle of 45° and a major diameter of 90 mm. A hemispherical forming tool having a diameter of 15 mm is used to produce the localised deformation. The initial configuration is shown in figure 2. In the numerical simulation, the forming tool is modelled as a rigid body, while the blank sheet is represented as an elastic-plastic deformable body using the material properties of aluminium alloy, Al-5251-H22. The elastic part of the constitutive behaviour of the sheet material is defined by a Young's modulus of 70 GPa and a Poisson ratio of 0.34. The plastic part of the material is assumed to be isotropic with the stress-strain curve described by, $\sigma = 390\varepsilon^{0.19}$ MPa, and an initial yield stress of 165 MPa. Where, σ is the flow stress and ε is the plastic strain. The density of the sheet material is 2700 kg/m^3. For simplicity, anisotropic, thermal and rate effects are not included in the present model.

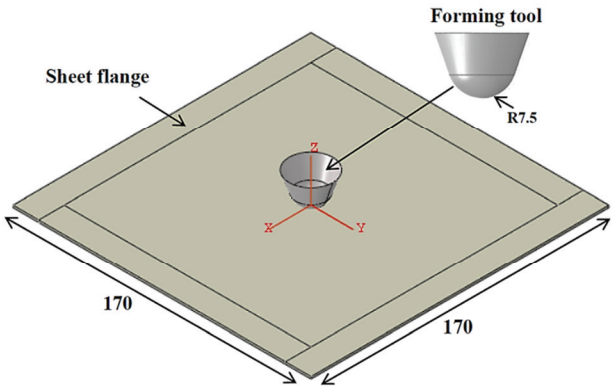

Fig. 2. *The configuration of the full, first-level, 3-D FE model of SPIF to produce a truncated cone (dimensions in mm).*

2.2. Boundary conditions

The initial sheet blank is completely fixed at the sheet flange where it is constrained by displacement boundary conditions such that it cannot move in any of the XYZ directions. The flange is clamped to give a smaller region of 150 mm x 150 mm free to deform. These settings reproduce the experimental setup that will be discussed in section 3. The tool paths for the forming tool are generated using Matlab software and applied in Abaqus/CAE. The forming tool is assigned to move at 30 mm/s in the cartesian XYZ axes along the prescribed tool path and is free to rotate about its own axis. The tool path is principally a complete circular path through 360º followed by a downward translation of 1mm. The radius of the circular path reduces each time the tool moves down, also by 1 mm. 'Surface to surface' contact between the forming tool and sheet surface is assumed in the Abaqus model and coulomb friction is set with a low friction coefficient of 0.05. The tool does not rotate about its own axis in the FE model. At the end of the simulation, the forming tool moves freely to its original position and the boundary conditions of the sheet edges and clamped regions are removed. This allows springback to be assessed.

2.3. Finite element mesh

The initial sheet was meshed with 17298 elements (8-node solid element with reduced integration and hourglass control, C3D8R) with two elements through the thickness. All simulations were performed using Abaqus/Implicit on an Intel® CoreTM Dual computer with a 3GHz CPU. An assessment of the influence of different element types is given in section 3.1.

3. DISCUSSION AND VALIDATION OF THE FIRST-LEVEL FE MODEL RESULTS

Figure 3 shows the truncated cone at the end of deformation and the corresponding Von Mises stress distribution. Zero stress is indicated at the flange where the sheet is completely fixed. Adjacent to this region, a slight increase in the stress value can be seen as a result of the global bending. A uniform distribution develops along the cone wall with higher values found at the last tool path as a result of the materials reducing ability to unload at the end of deformation.

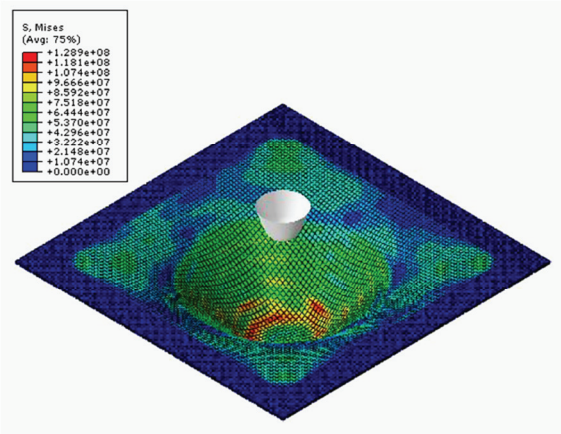

Fig. 3. *Von Mises stress (Pa) distribution in the fully deformed truncated cone.*

The sheet geometry indicated by the FE model was verified against a part produced on the Cambridge AISF machine (Allwood et al., 2005). This is a three-axis computer numerically controlled (CNC) machine purpose-built for the AISF process, see figure 4(a). The test product, which is shown in figure 4(b), was formed using 5251-H22 aluminium alloy.

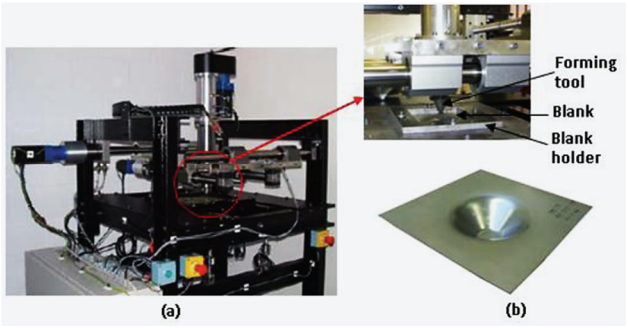

Fig. 4. *(a) AISF machine designed by Allwood et al. (2005) at the Cambridge University Institute for Manufacturing, (b) test product.*

3.1. Profile and thickness distributions

The profile of the truncated cone was measured using a 3-D coordinate measuring machine. The FE model with C3D8R elements predicts the observed sheet bending close to the major diameter of the cone, the springback at the cone base and the pillow effect at the centre of the cone, figure 5, a feature also observed by Micari et al. (2007). Analyses were also performed with alternative element types to assess their suitability, including a 4-node shell element with reduced integration (S4R), an 8-node continuum shell element with reduced integration (SC8R) and a fully integrated 8-node solid element (C3D8). Figure 5 shows that the 8-node solid elements (C3D8R) provided a more accurate reproduction of the experimental profile.

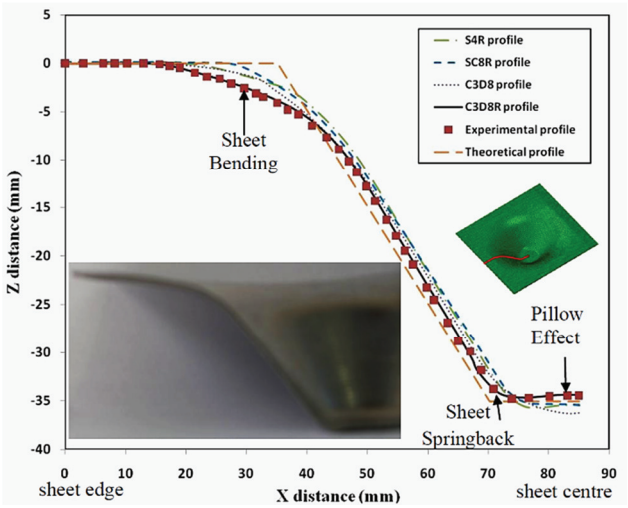

Fig. 5. *The profile plots of a 45° truncated cone, showing FE results for different element types and experimental data.*

After the profile was measured an electro-discharge cutting machine was used to cut the formed part along the central plane and the sheet thickness determined. Figure 6 shows the thickness variation obtained by FE analyses with different element types, experimental measurements and for comparison, by an analytical technique. The latter was obtained by applying the well-known sine law ($t_f = t_0 \sin\theta$) (Hussain & Gao, 2007). It can be seen that the sheet thinning increases as the cone depth increases, while near to the cone base, less thinning is apparent. For a distance between 50 mm and 70 mm from the sheet edge, the sheet thickness remains almost constant at 0.70 mm, and at the cone base, the sheet thickness is closer to its original value. While all the FE analyses reproduced the general trend, figure 6 confirms that the simulation conducted using the C3D8R elements most closely matched

the experimental data and these elements were therefore used for all further analyses presented here. The suitability of solid elements for SPIF modelling has also been demonstrated by Ma and Mo (2008) and by Eyckens et al. (2010).

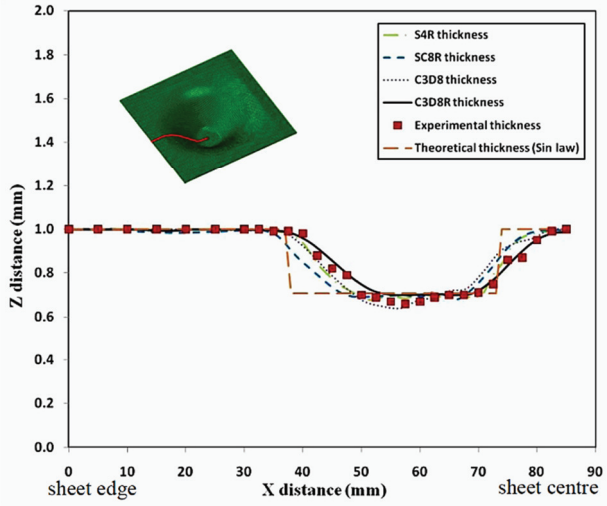

Fig. 6. *Thickness distribution along central plane of the 45º truncated cone, showing FE results for different element types and experimental data.*

3.2. Forming force components

During the forming process, three force components F_x, F_y and F_z are recorded as shown in figure 7. F_x and F_y are those components in the plane of the tool's circular path while F_z is the tool force in the vertical direction. In the first complete path, all forces are almost zero. For any subsequent complete path, F_x and F_y have a similar, i.e. trend and reach their maximum and minimum values in a sinusoidal manner. F_x decreases for the first 90º of tool movement to reach its minimum value at this position. It then starts to increase and becomes zero again at 180º and continues to increase until its maximum value is reached at 270º, after which it decreases again and becomes zero when the tool returns to its original position. F_y has the opposite trend of F_x. F_z incrementally increases as the accumulated downward translation of the tool increases with much higher peak values than F_x and F_y. Figure 7 shows a comparison between the FE forces and the experimental forces. In order to simplify the graph, the average amplitude of the experimental force F_z and the maximum amplitude of the experimental forces F_x, F_y (the averages being zero) are displayed. As the cone depth increases, the peak values of F_x, F_y and F_z increase until maximum plastic deformation after which the forces stabilise at approximately 280 N and 630 N respectively. Similar trends have been observed by Duflou et al. (2007).

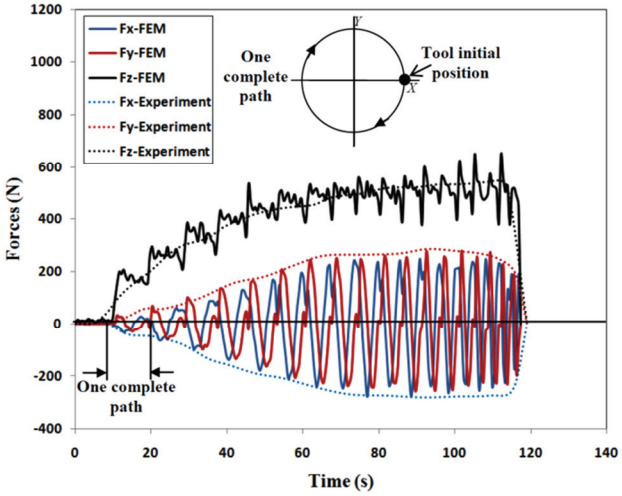

Fig. 7. *Development of the three force components.*

3.3. Stress and strain distributions

The deformation history shown in figures 8, 9 and 11, is divided into three regions; (a) the commencement of deformation, (b) mid-way through the process and (c) at the end of the process. After initial tool contact, figure 8(a), the Von Mises stress is localised principally beneath the tool while the rest of the sheet deforms elastically. Due to the evolution of deformation induced by the tool movement, out-of-plane distortion develops as the sheet adopts a more three-dimensional geometry. This, together with further plastic deformation, provides a more rigid behaviour and restricts the elastic recovery of the material away from the contact region.

The localised peak stress areas are clearly defined by the annular regions shown in figures 8(b) and 8(c) which develop along the tool path that has just completed. At the end of the process there is a small variation from the inner edge of the flange region to the highly localised region at the last tool path.

Figure 9 shows the evolution of equivalent plastic strain through the deformation. There is clearly no plastic deformation at the beginning of the process as shown in figure 9(a). Plastic strains are generated as the tool moves across the sheet, associated with the combined stretching and bending behaviour, figure 9(b). As a result of increasing the deformation depth, the plastic strain gradually increases over the cone wall and attains its maximum value near to the cone base. It decreases again after the maximum sheet thinning and reduces to zero at the cone base as shown in figure 9(c).

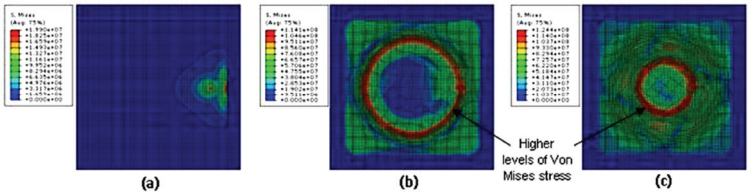

Fig. 8. Von Mises stress (Pa) distributions, at (a) the commencement of deformation, (b) mid-way through the process and (c) at the end of the forming process.

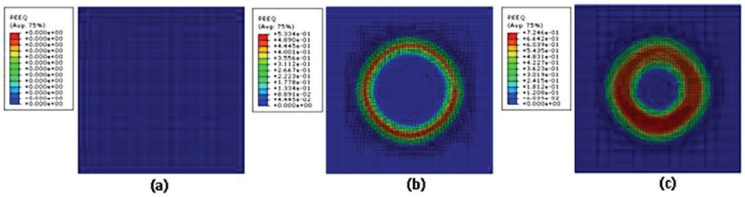

Fig. 9. Evolution of plastic strain, at (a) the commencement of deformation, (b) mid-way through the process and (c) at the end of the forming process.

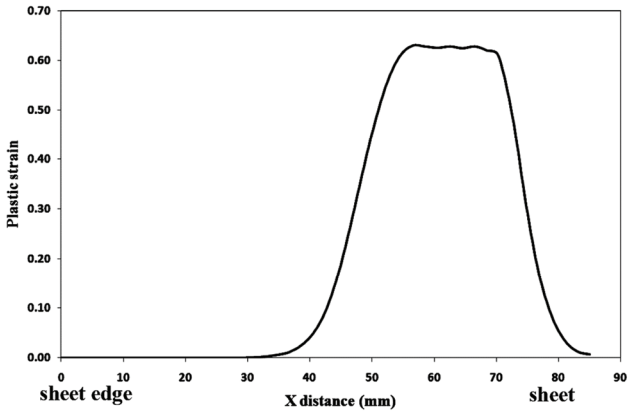

Fig. 10. Plastic strain distribution along a central plane of the 45° truncated cone.

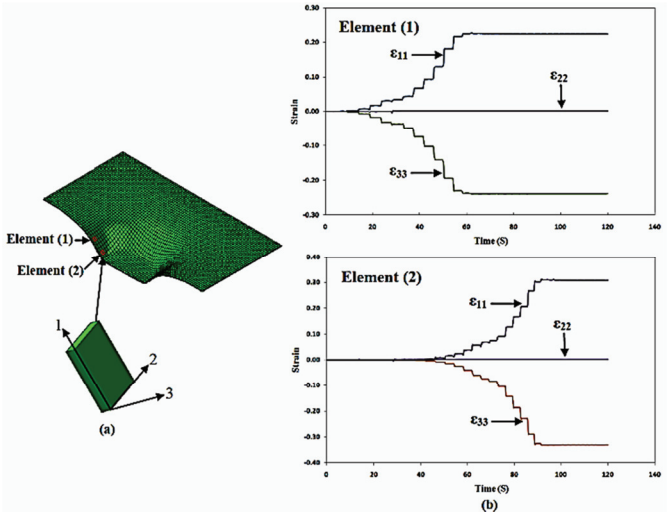

Fig. 12. (a) Two control elements along the cone wall, (b) strain history on the control elements.

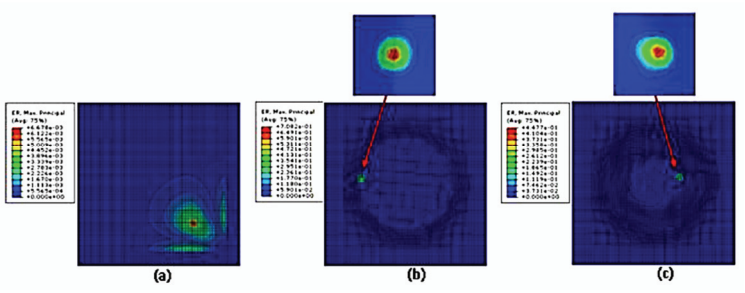

Fig. 11. Evolution of strain rate (s-1), at (a) the commencement of deformation, (b) mid-way through the process and (c) at the end of the forming process.

This can be confirmed from the plastic strain distribution along the central plane of the cone shown in figure 10. At the sheet flange, the plastic deformation is zero where the sheet is completely fixed in this region. The plastic deformation then starts to increase and the maximum corresponds to the maximum sheet thinning which takes place along the 45° wall angle (see figure 6). After this peak, the plastic deformation decreases towards the centre of the sheet.

From the total strain rate distribution shown in figure 11(a), there is a wide area of sheet bending around the tool at the beginning of deformation. As the process progresses, the deformation becomes more localised at the contact region beneath the forming tool which clearly demonstrates the incremental nature of the process as shown in figure 11(b) and 11(c).

3.4. History of strain components

To demonstrate the strain component history through the process, two elements on the upper surface of the cone are selected (figure 12a). One is located at the middle upper region of the cone wall and the other at the lower region near to the cone base. The strain components are measured with respect to a local coordinate system, where ε_{11}, ε_{22} and ε_{33} are the strain components equivalent to the radial, circumferential and axial directions respectively, figure 12(a). Only the

components in the 1-3 plane, ε_{11}, ε_{33} have significant values while ε_{22} is almost zero, (figure 12b), which indicates near plane-strain deformation. It can be seen that the sheet stretching associated with ε_{11} and sheet thinning associated with ε_{33}, combined with sheet bending next to the sheet flange, are the dominant modes of deformation. The values of the radial and axial strain components clearly increase as the forming progresses. No further strain is imposed once the forming tool moves out of contact with the element and on to a subsequent path. However, while the full model predicts the history of the normal strain components, the use of two elements through the sheet is not sufficient to obtain accurate data on through-thickness shear strains.

4. METHODOLOGY FOR THE DUAL-LEVEL FINITE ELEMENT MODEL

In order to predict the through-thickness shear strains which are believed to be the main contribution to the high forming limits typical of this process, a model with a sufficient number of elements through the thickness must be constructed. For the full FE model presented above, a large number of elements, i.e. more than three, will result in very long, unrealistic simulation times, of the order of several days or more for each simulation. Therefore, it is necessary to use a dual-level approach. In this technique the full model is run only until sufficient deformation, typical of the whole process, has occurred. A second-level FE model is then created in which a large number of elements can be assigned through the thickness.

These requirements can be fulfilled through the following procedure: The full model is to be simulated for a number of successive loops of tool movement until a sufficient amount of plastic strain is generated. This could be established qualitatively. A segment of the sheet that surrounds the forming tool and includes deformed and un-deformed regions is then extracted. For this second-level FE model, the geometry of the full model including the last position of the forming tool is applied and a larger number of elements through the thickness is assigned. In the second-level FE model, the deformation process should continue exactly as in the full model.

4.1. Example of dual-level approach

This procedure can be demonstrated with a simple generic example, which is used also to determine the minimum number of elements required through the sheet thickness. An FE model for the SPIF process was constructed using a sheet strip of 80 mm length, 50 mm width and 1 mm thickness. The sheet end faces are constrained by displacement boundary conditions such that they cannot move in the X-direction and the side faces cannot move in the Y-direction (figure 13). The tool is free to move corresponding to the tool path. The tool movement is principally a complete linear path along the Y-direction followed by a downward translation along the X-Z plane, after which the Y-translation is repeated. The sheet was meshed with 2 elements through the thickness and a total of 3102 solid elements, type C3D8R. The process of constructing the second-level FE model is shown in figure 13. After three successive tool paths, a partially deformed 30mm x 15mm segment of sheet was extracted as shown in figure 13(a) and (b). The dimensions of the selected segment were obtained after preliminary trials. The target was to find the minimum dimensions that allowed a sufficient amount of tool movement and deformation. The current nodal coordinate points of the selected piece were extracted from the model data and used to define the bounding surfaces within which a new body, as shown in figure 13(c), could be created. A new second-level FE model using this geometry was then constructed (figure 13d) and meshed with linear solid elements.

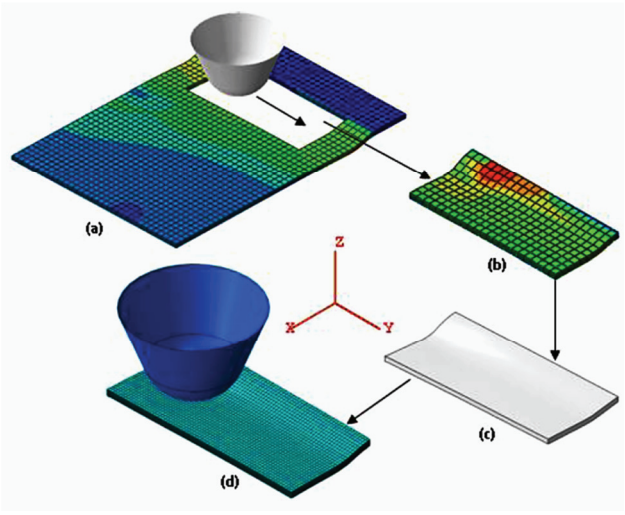

Fig. 13. *An example of the process of constructing the second, lower level, FE model.*

The forming tool was modelled as a rigid body with a 15 mm diameter hemisphere and placed at the last position attained in the original model. The tool is again prescribed to move parallel to the sheet in the Y-direction. The same boundary conditions of the strip model are applied to the new FE model.

Since the segment was removed near to the beginning of deformation, the amount of generated stresses and strains are very small compared to those at the end of deformation, and any initial stresses or strains were therefore ignored.

4.2. Influence of number of through-thickness elements

In order to assess the influence of changing the number of elements through the sheet thickness the maximum value of shear strain γ_{23} was selected as the main criterion. This was expected to show the most significant contribution of the strain components. As the number of through-thickness elements increased, the maximum value of the shear strain γ_{23} also increased, figure 14. However, increasing the number of elements beyond seven showed very little effect as the value began to converge. Seven elements through the thickness were therefore used in all subsequent analyses. Figure 14 also shows the significant increase in simulation time for each model.

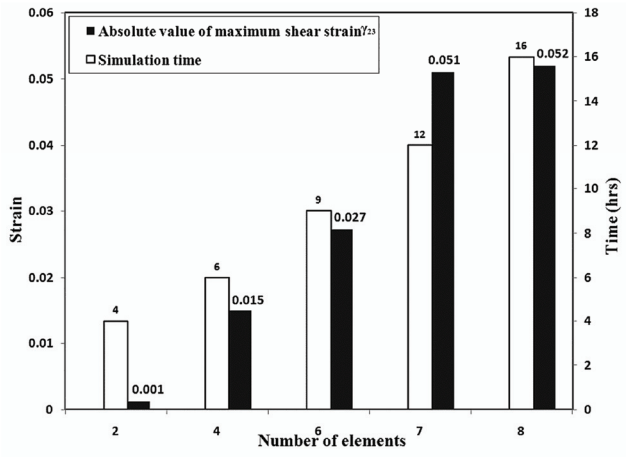

Fig. 14. Effect of number of elements through the sheet thickness on the maximum value of shear strain γ_{23} and simulation time.

The need to use a sufficient number of elements is confirmed by an examination of the strain components for an element in the centre of the sheet, originally under the tool at the beginning of the process. Figure 15 shows the strain history obtained at the end of deformation with two elements through the sheet, while figure 16 shows the strain history obtained from the more refined second-level FE model. The strain components ε_{11}, ε_{22} and ε_{33} are similar in both cases, but there are clear differences in the shear strain components γ_{13} and γ_{23}. γ_{13} is the shear strain in the plane perpendicular to the tool movement and results from pushing the forming tool across the material along the wall angle. It first increases incrementally until it reaches a steady value and then remains constant. Strain component γ_{23} is the shear component in the plane parallel to the tool movement and is principally a result of the friction between the forming tool and the sheet surface. The maximum value of this shear strain is much higher than the other components, which could contribute to a higher forming limit in the SPIF process. Shear strain component γ_{12} has no contribution.

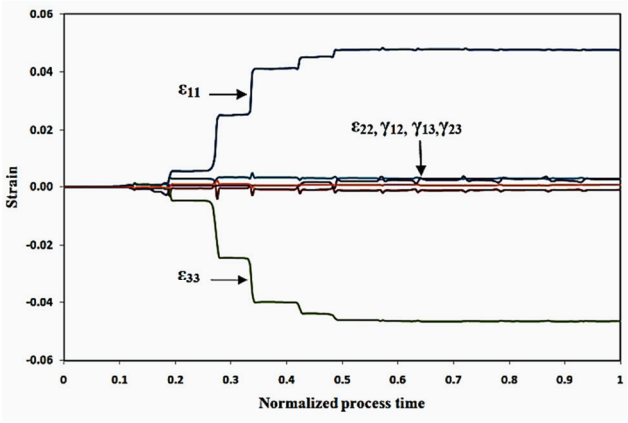

Fig. 15. Strain history obtained using the first-level FE model from the example case at the end of deformation with 2 elements through the sheet thickness.

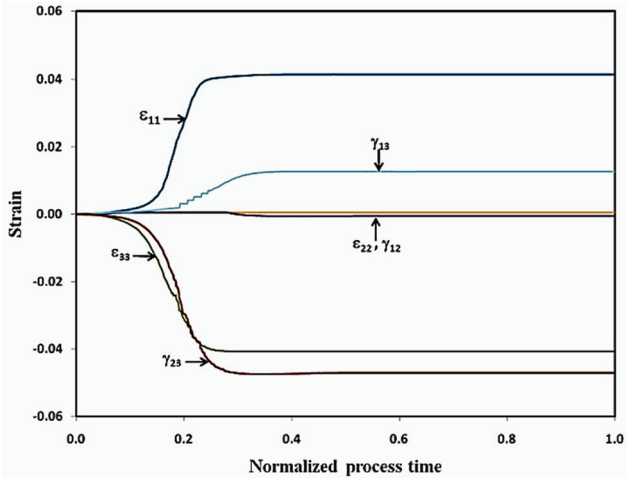

Fig. 16. Strain history on an element in the middle of the sheet thickness of the second-level FE model with 7 elements through the sheet thickness.

5. A REFINED SECOND-LEVEL FE MODEL FOR A TRUNCATED CONE

Having demonstrated the effectiveness of the two-level FE strategy for a simple case, the same approach is now applied to the forming of the truncated cone. The process is illustrated in figure 17. After three successive paths of deformation in the full model, a 55 mm x 55 mm segment of the sheet

was extracted. After extracting the nodal coordinate points of this segment, the surfaces defined the boundary of the new model, as shown in figure 17(c), within which the second-level FE mesh was created. This model was meshed with 7 elements (type C3D8R) through the thickness, with a total of 25137 elements, as shown in figure 17(d). The forming tool is set to move a distance of 25mm along an arc at the same speed as in the full model.

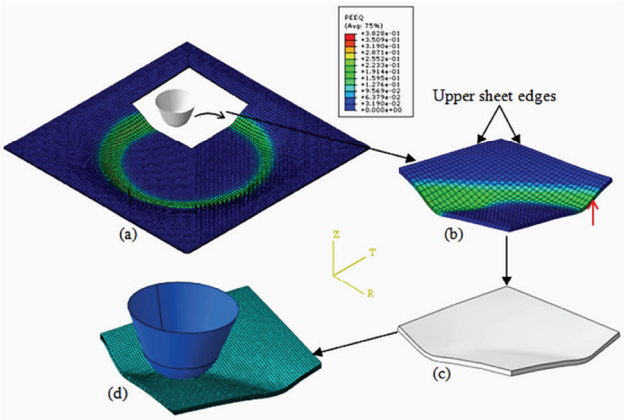

Fig. 17. *The four stages in the process of constructing the second level FE model for a truncated cone.*

5.1. Boundary conditions in the second level model

The boundary conditions in the smaller segment must reproduce, as close as possible, the sheet behaviour in the full model. The size of the segment was chosen after preliminary trials (Essa, 2011) to ensure that the tool trajectory and the elements selected for a more detailed examination were sufficiently far from the segment edges to minimise any minor differences in boundary effects. The two outer edges of the segment near to the original outer edges of the sheet were selected to coincide with the limits of the mesh in the full model beneath the clamped region. The nodes on these edges, in both the full (first-level) and in the segment (second-level) were constrained so that there was no movement in the vertical, Z-direction. The experimental measurements showed no reduction in thickness in this region of the sheet. If the edges of the segment were not coincident with the edges of the clamped region then different boundary conditions, consistent with any local displacement would be required. The other two side edges of the segment are constrained so that any nodal displacement occurs either in the R-Z or T-Z planes as appropriate. In order to establish the suitability of these constraints, the displacements of nodal points on the two faces in the reduced segment, and at the corresponding locations in the full model were checked. One example for a node (indicated by the arrow in figure 17) is given in figure 18, which shows a typical correlation between the edge displacements and demonstrates the suitability of the boundary conditions imposed.

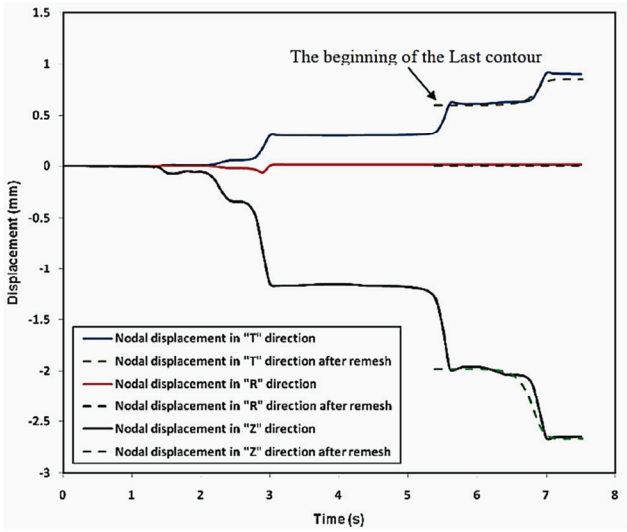

Fig. 18. *Comparison of node displacements in the first and second level models for a selected nodal point, the selected node is from the region indicated by the arrow in figure 17.*

5.2. Stress and strain in the cone forming process

The Von Mises stress distribution in the second-level model, is shown in figure 19(a), with the distinct annulus of high localised stresses developing and very little deformation in the remainder of the sheet, consistent with the full model. A cross-section along the T-Z plane, located near to the initial tool position, shown in figure 19(b), illustrates the shear deformation through the thickness. The enlarged view in figure 19(c) highlights the significant shear deformation compared to the elements in the undeformed region. It shows the shear deformation in the 1-3 plane, γ_{13}, and in the 2-3 plane, γ_{23} for this set of elements. A control element in the middle of this set, as shown in figure 19(c), is selected from which to extract the strain history.

The strain history of the selected element is shown in figure 20. Two shear strain components γ_{13} and γ_{23}, in addition to the normal strain components ε_{11} and ε_{33}, are clearly revealed as a result of increasing the number of elements through the thickness. The shear strain γ_{23} has the greatest magnitude with no contribution from the normal strain component ε_{22} and shear strain component γ_{12}. The distributions of the shear strains γ_{13} and γ_{23} through the thickness are shown in figure 21. The maxima are found at the

top surface in contact with the tool, reducing to small values at the opposing surface. These findings in general agree with the experimental results obtained by Allwood et al. (2007) and Jackson and Allwood (2009).

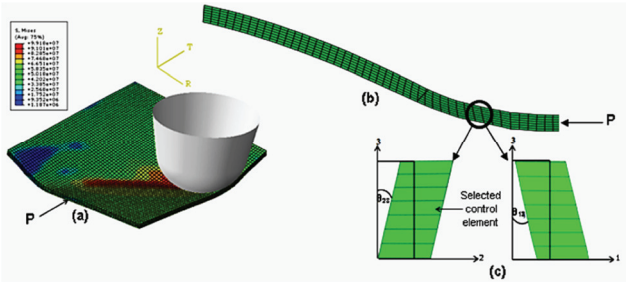

Fig. 19. *(a) Von Mises stress (Pa) distribution, (b) edge view in the T-Z (1-3) plane near the initial tool position and (c) illustration of shear deformation.*

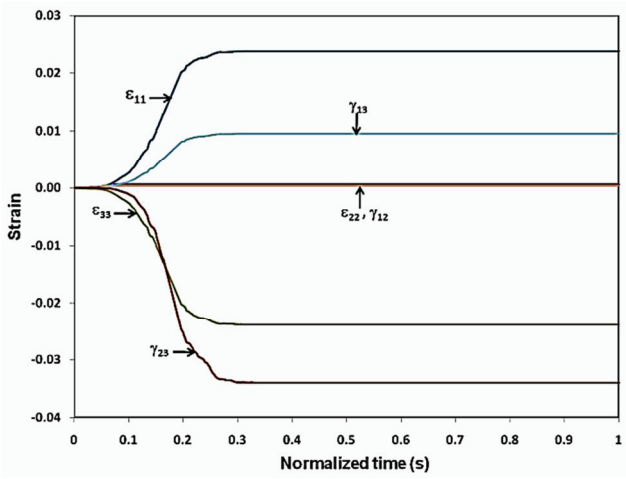

Fig. 20. *Strain history of the second-level FE model of the truncated cone.*

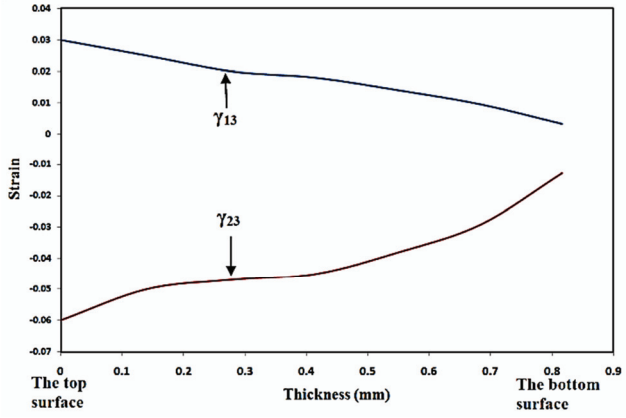

Fig. 21. *Shear strain distribution along the sheet thickness of the second-level FE model of the truncated cone.*

Quantitative comparisons to experimental data are not possible due to the scarcity of such information. Two different experimental techniques have been made to determine through-thickness shear, but both acknowledge limitations of the experimental procedure and describe them only as qualitative indications of shear. For example, Jackson and Allwood (2009), estimated through-thickness shear by measuring the relative displacement of points marked on the upper and lower surfaces of two copper half-plates brazed together to form a complete sheet. The grid lines on the mating surfaces were measured after deformation to give an indication of the shear. In global terms, they found significant shear strain in planes 1-3 and 2-3. Their results were obtained along the central plane of the sheet surface of the fully deformed part. Eyckens (2010) estimated the through-thickness shear strain by deforming aluminium AA3103 sheets with small holes, aligning upper and lower deformed ellipses to give an indication of average shear across the sheet. It is suggested that it is difficult to determine accurately, how much of the shear is produced by the presence of the holes. General trends of average through-thickness shear are similar to those observed here.

5.3. Influence of friction and tool diameter on shear strain

The development of the dual-level methodology provided the opportunity to assess the influence of process parameters on the shear strain distribution through the sheet. In the cone forming process the interface friction and tool diameter were considered. In the case of friction, three coefficients of 0.05, 0.26 and 0.5 were used (each with a tool diameter of 15 mm). Tool diameters of 10, 15 and 20 mm were assessed (each with a friction coefficient of 0.26). Allwood et al. (2007) and Jackson and Allwood (2009) reported that the process formability is strongly influenced by the through-thickness shear strains, and these could be increased by increasing the friction between the forming tool and sheet surface. The influence of friction in the present model is shown in figure 22. With a low value of friction, 0.05, the variation in shear strain γ_{23}, across the sheet is less than the variation in γ_{13}. When the friction is increased the γ_{13} component changes very little and a similar variation is observed, but at a slightly lower magnitude. The effect of friction on the γ_{23} component is much more pronounced. Not only does the gradient across the sheet increase, but also the magnitude significantly increases. For example, at the upper surface in contact with the tool, it is 0.06 for a coefficient of 0.05, 0.15 for a coefficient of 0.26 and 0.27 for the higher coefficient of 0.5. This con-

firms that increasing friction will increase shear strain, however, Hussain et al. (2008a) have shown that high friction will result in undesirable surface roughness so care must be exercised when increasing friction.

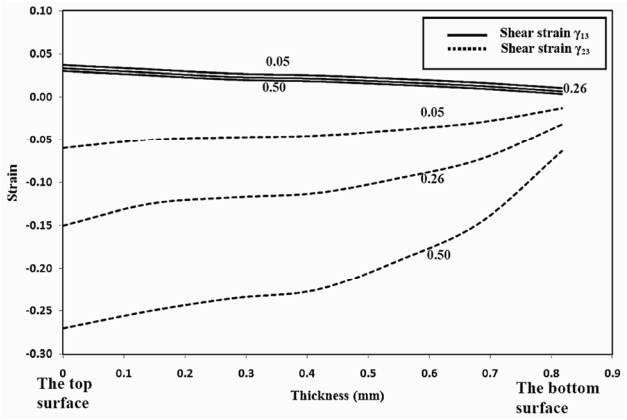

Fig. 22. *Effect of friction coefficient on the through-thickness shear strain.*

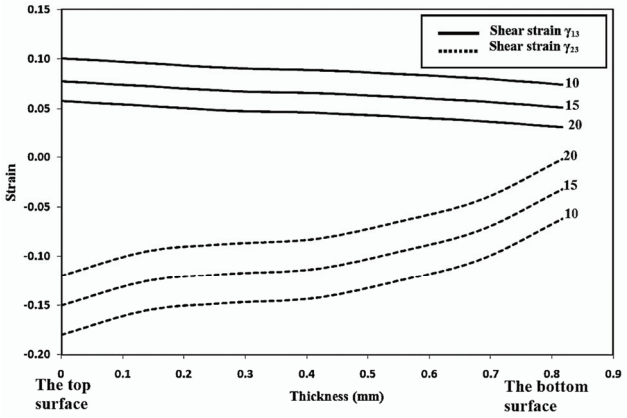

Fig. 23. *Effect of tool diameter on the through-thickness shear strain.*

Using a small diameter tool tends to localise the deformation underneath the tool and increase the strains. As the tool diameter increases, the contact area increases and hence the contact pressure decreases. As a result of increasing the contact area, the deformation becomes more distributed and hence the forming forces decrease which leads to a decrease in the strains that are generated. Figure 23 shows clearly that the magnitude of the shear strain reduces as the tool diameter is increased, although the gradient across the sheet remains unchanged. Ham and Jeswiet (2006), Hussain et al. (2008b) and Le et al. (2008) have reported that as the tool diameter decreases the process formability increases, consistent with an increase in shear deformation.

6. CONCLUSIONS

A dual-level finite element model for single point incremental forming processes has been developed and implemented using the Abaqus/Implicit code. The full, first-level, FE model results were compared to and validated against experimental data. The FE results showed good correlation with the profile, thickness distribution and force history from experimental measurements. The second-level FE model based on a segment of the original model, showed the importance of assigning a sufficient number of elements through the thickness to provide a more comprehensive study on shear effects in the SPIF process.

This study demonstrated the following,

- The full FE model was capable of predicting the final part geometries and dimensions in addition to the force history and normal strain evolution.
- The full model showed that stretching, thinning and bending were the dominant modes of deformation in SPIF.
- In order to explore through-thickness modes of deformation, a large number of elements through the thickness were required and thus, the full model was not suitable.
- The second-level FE model revealed a significant magnitude of the through-thickness shear strains on planes perpendicular to and parallel to the tool movement, the greatest shear appearing on the former.
- An increase in tool friction had very little influence on the γ_{13} component, but increased both the magnitude and gradient of the γ_{23} component.
- Increasing the tool diameter reduced the magnitude of the shear strains but did not affect the through-thickness gradient.
- The development of the dual-level FE model will permit further research on the influence of various process parameters on through-thickness shear deformation.

ACKNOWLEDGEMENTS

The truncated cone test sample and the experimental force data were kindly provided by Julian Allwood and Omer Music of the Cambridge University Institute for Manufacturing. We are grateful for their valuable ideas and comments in developing the FE model described here. The financial support of

the UK ORSAS Scheme (K Essa) is gratefully acknowledged.

REFERENCES

Allwood, J., Houghton, N. E., Jackson, K., 2005, The Design of an Incremental Forming Machine, *SheMet '05, Proceedings of the 11th International Conference on Sheet Metal*, Erlangen, Germany, 471-478.

Allwood, J., Shouler, D. R., Tekkaya, A. E., 2007, The increased forming limits of incremental sheet forming processes, *Proceedings of the 12th International Conference on Sheet Metal*, Palermo, 621-628.

Ambrogio, G., Filice, L., Fratini, L., Micari, F., 2004, Process mechanics analysis in single point incremental forming, *Proceedings of the 8th International Conference on Numerical Methods in Industrial Forming Processes*, Columbus, Ohio, 922-927.

Bambach, M., Hirt, G., Junk, S., 2003, Modelling and experimental evaluation of the incremental CNC sheet metal forming process, *Proceedings of the 7th International Conference on Computational Plasticity*, Barcelona, 1-17.

Dejardin, S., Thibaud, S., Gelin, J.C., 2008, Finite element analysis and experimental investigations for improving precision in single point incremental sheet forming process, *International Journal of Material Forming*, 1, 121-124.

Duflou, J., Tunçkol, Y., Szekeres, A., Vanherck, P., 2007, Experimental study on force measurements for single point incremental forming, *Journal of Materials Processing Technology*, 189(1-3), 65-72.

Emmens, W. C., Van Den Boogaard, A. H., 2009, An overview of stabilizing deformation mechanisms in incremental sheet forming, *Journal of Materials Processing Technology*, 209(8), 3688-3695.

Essa, K., 2011, *Finite element prediction of deformation mechanics in incremental forming processes*, PhD Thesis, University of Birmingham.

Eyckens, P., 2010, *Formability in Incremental Sheet Forming: Generalization of the Marciniak-Kuczynski Model*, Doctor of Engineering Thesis, Katholieke Universiteit Leuven.

Eyckens, P., He, S., Van Bael, A., Van Houtte, P., Duflou, J.R., 2007, Forming limit predictions for the serrated strain paths in single point incremental sheet forming, *Proceedings of Numiform 07, the 9th International Conference on Numerical Methods in Industrial Forming Processes*, Porto, 141-146.

Eyckens, P., Van Bael, A., Aerens, R., Duflou, J. R., Van Houtte, P., 2008, Small-scale finite element modelling of the plastic deformation zone in the incremental forming process, *International Journal of Material Forming*, 1, 1159-1162.

Eyckens, P., Belkassem, B., Henrard, C., Gu, J., Sol, H., Habraken, A.M., Duflou, J.R., Van Bael, A., Van Houtte, P., 2010, Strain evolution in the single point incremental forming process: digital image correlation measurement and finite element prediction, *International Journal of Material Forming*, 4, 1, 55-71.

Hadoush, A., Van Den Boogaard, A. H., 2008, Time reduction in implicit single point incremental sheet forming simulation by refinement - derefinement, *International Journal of Material Forming*, 1, 1167-1170.

Hadoush, A., Van Den Boogaard, A., 2009, Substructuring in the implicit simulation of single point incremental sheet forming, *International Journal of Material Forming*, 2(3), 181-189.

Ham, M., Jeswiet, J., 2006, Single Point Incremental forming and the forming criteria for Aa3003, *CIRP Annals - Manufacturing Technology*, 55(1), 241-244.

Hirt, G., Bambach, M., Junk, S., 2003, Modelling of the incremental CNC sheet metal forming process, *Proceedings of the 10th International Conference on Sheet Metal*, Belfast.

Hussain, G., Gao, L., 2007, A novel method to test the thinning limits of sheet metals in negative incremental forming, *International Journal of Machine Tools and Manufacture*, 47(3-4), 419-435.

Hussain, G., Gao, L., Zhang, Z., 2008a, Formability evaluation of a pure titanium sheet in the cold incremental forming process, *The International Journal of Advanced Manufacturing Technology*, 37(9), 920-926.

Hussain, G., Hayat, N., Gao, L., 2008b, An experimental study on the effect of thinning band on the sheet formability in negative incremental forming, *International Journal of Machine Tools and Manufacture*, 48(10), 1170-1178.

Jackson, K., Allwood, J., 2009, The mechanics of incremental sheet forming, *Journal of Materials Processing Technology*, 209(3), 1158-1174.

Lasunon, O., Knight, W., 2007, Comparative investigation of single-point and double-point incremental sheet metal forming processes, *Proceedings of the Institution of Mechanical Engineers, Part B: Journal of Engineering Manufacture*, 221(12), 1725-1732.

Le, V., Ghiotti, A., Lucchetta, G., 2008, Preliminary studies on single point incremental forming for thermoplastic materials, *International Journal of Material Forming*, 1, 1179-1182.

Ma, L. W., Mo, J. H., 2008, Three-dimensional finite element method simulation of sheet metal single-point incremental forming and the deformation pattern analysis, *Proceedings of the Institution of Mechanical Engineers, Part B: Journal of Engineering Manufacture*, 222(3), 373-380.

Micari, F., Ambrogio, G., Filice, L., 2007, Shape and dimensional accuracy in single point incremental forming: state of the art and future trends, *Journal of Materials Processing Technology*, 191(1-3), 390-395.

Park, K., Yang, D. Y., 2000, Mismatching refinement with domain decomposition for the analysis of steady-state metal forming process, *International Journal for Numerical Methods in Engineering*, 48(7), 1089-1106.

Quigley, E., Monaghan, J., 2002, The finite element modelling of conventional spinning using multi-domain models, *Journal of Materials Processing Technology*, 124(3), 360-365.

Robert, C., Dal Santo, P., Delamézière, A., Potiron, A., Batoz, J. L., 2008, On some computational aspects for incremental sheet metal forming simulations, *International Journal of Material Forming*, 1, 1195-1198.

Tanaka, S., Nakamura, T., Hayakawa, K., Nakamura, H., Motomura, K., 2007, Residual stress in sheet metal parts made by incremental forming process, *Proceedings of Numiform 07, the 9th International Conference on Numerical Methods in Industrial Forming Processes*, Porto, 775-780.

OCENA METODĄ DWUPOZIOMOWĄ ELEMENTÓW SKOŃCZONYCH ZMIAN MECHANIZMU ODKSZTAŁCENIA NA GRUBOŚCI W JEDNOPUNKTOWYM PRZYROSTOWYM KSZTAŁTOWANIU BLACH

Streszczenie

Jednopunktowa przyrostowa metoda kształtowania blach (ang. single point incremental forming - SPIF) jest procesem umożliwiającym uzyskiwanie skomplikowanych kształtów przy zastosowaniu prostych narzędzi. Nie jest potrzebna zgodność kształtu narzędzia i wyrobu. Stosowane obecnie modele tego procesu nie określają jednoznacznie zmian odkształcenia i ścinania na grubości blachy. Cele niniejszej pracy to po pierwsze opracowanie metody analizy mechanizmów odkształcenia w SPIF, a po drugie dostarczenie opisu schematów odkształcenia występujących w tym procesie wzdłuż grubości blachy. Zastosowano metodę podejścia wielopoziomowego, chociaż w rozważanym zadaniu potrzebne były tylko dwa poziomy. Dla kształtowanej blachy wykorzystano model implicit 3D na bazie metody elementów skończonych (MES), z dwoma elementami na grubości. Dla małego wycinka blachy zastosowano model MES drugiego poziomu z siedmioma elementami na grubości. Wyniki wykazały, że pełny model umożliwia ocenę tylko głównych charakterystyk odkształcenia, czyli odkształceń normalnych i kształtu wyrobu. Model drugiego poziomu przewiduje dokładniej schemat odkształcenia na grubości blachy i umożliwia ocenę wpływu tarcia i średnicy na rozkład odkształceń postaciowych wzdłuż grubości. Dodatkowo możliwy był opis połączonego wpływu zginania, rozciągania i pocienienia. W konsekwencji uzyskane wyniki dostarczają pełniejszego opisu mechanizmów odkształcenia na grubości blachy

Received: October 12, 2011
Received in a revised form: January 24, 2012
Accepted: February 02, 2012